ACS OMEGA

http://pubs.acs.org/journal/acsodf

Article

Density Functional Theory Analysis of Structural, Electronic, and Optical Properties of Mixed-Halide Orthorhombic Inorganic Perovskites

Hamid M. Ghaithan,* Zeyad. A. Alahmed,* Saif M. H. Qaid, and Abdullah S. Aldwayyan*

Cite This: *ACS Omega* 2021, 6, 30752−30761

Read Online

ACCESS | Metrics & More | Article Recommendations | Supporting Information

ABSTRACT: Inorganic metal-halide perovskites hold a lot of promise for solar cells, light-emitting diodes, and lasers. A thorough investigation of their optoelectronic properties is ongoing. In this study, the accurate modified Becke Johnson generalized gradient approximation (mBJ-GGA) method without/with spin orbital coupling (SOC) implemented in the WIEN2k code was used to investigate the effect of mixed I/Br and Br/Cl on the electronic and optical properties of orthorhombic $CsPb(I_{1-x}Br_x)_3$ and $CsPb(Br_{1-x}Cl_x)_3$ perovskites, while the Perdew−Burke−Ernzerhof generalized gradient approximation (PBE-GGA) method was used to investigate their structural properties. The calculated band gap (E_g) using the mBJ-GGA method was in good agreement with the experimental values reported, and it increased clearly from 1.983 eV for $CsPbI_3$ to 2.420 and 3.325 eV for $CsPbBr_3$ and $CsPbCl_3$, respectively. The corrected mBJ + SOC E_g value is 1.850 eV for $CsPbI_3$, which increased to 2.480 and 3.130 eV for $CsPbBr_3$ and $CsPbCl_3$, respectively. The calculated photoabsorption coefficients show a blue shift in absorption, indicating that these perovskites are suitable for optical and optoelectronic devices.

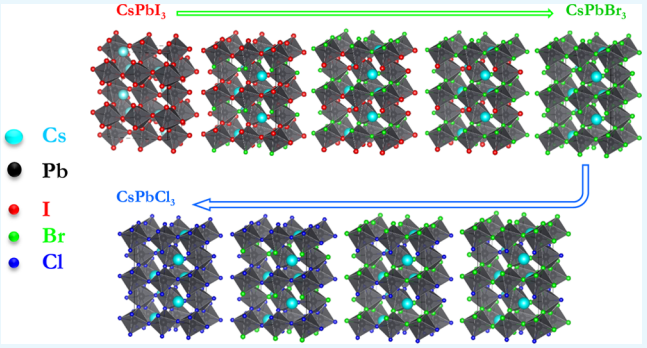

1. INTRODUCTION

Because of their superior thermal stability compared to their organic−inorganic hybrid counterparts, inorganic perovskites have emerged as one of the most appealing research hotspots in the field of perovskite photovoltaics over the last 5 years.[1−3] Perovskite compounds have the chemical formula ABX_3, where A is a monovalent cation such as CH_3NH_3 (MA), $HC(NH_2)_2$ (FA), or Cs, B is a divalent cation such as Pb or Sn, and X is an anion such as I, Br, or Cl.[4] Inorganic mixed halides have recently been used to create various nanophotonic components due to their electroluminescence in the green[5,6] to blue[7] optical ranges. The broad tunability of halide perovskites has emerged as promising demonstrations for appealing solar cells, light-emitting diodes (LEDs), and laser applications, with the possibility of manipulating energy-efficient fluorescent lighting by replacement of the cations (MA, FA, and Cs) or halide components (I, Br, and Cl).[8] Numerous density functional theory (DFT) calculations have been performed in recent years to investigate the structural, electronic, and optical properties of organic−inorganic perovskites.[4,9−32] The local density approximation (LDA) method was used to conduct theoretical studies of organic−inorganic perovskites[33] or Perdew−Burke−Ernzerhof generalized gradient approximation (PBE-GGA)[34,35] as a result of their low computational cost.[36] Because the obtained E_g values were much lower than the experiment values, the LDA and PBE-GGA potentials were unable to calculate the accurate E_g.[34,35,37−39] Furthermore, the theoretical lattice parameters calculated with PBE-GGA outperformed the experimental lattice constants.[36] The LDA potential typically underestimated the lattice constants, resulting in an underestimation of E_g.[36] To overcome the significant shortcomings of the LDA and PBE-GGA potentials, our previous work demonstrated that the modified Becke Johnson (mBJ-GGA) potential is the most accurate method for studying the optoelectronic properties of $CsPbBr_3$ perovskites.[40] Because of its additional dependence on the kinetic energy density, the mBJ-GGA potential can be used to calculate E_g with good agreement with experimental values.[41−44] Structural and electronic properties of mixed inorganic cubic symmetry at higher temperature were studied using DFT-based full-potential linear augmented plane wave (FP-LAPW) approach.[23,45,46] Chen et al. studied the electronic band gaps for a 1 × 1 × 2 supercell of $CsPb(I_{1-x}Cl_x)_3$ and $CsPb(I_{1-x}Br_x)_3$ cubic phases at higher temperature.[23,45,46]

Received: September 1, 2021
Accepted: October 26, 2021
Published: November 5, 2021

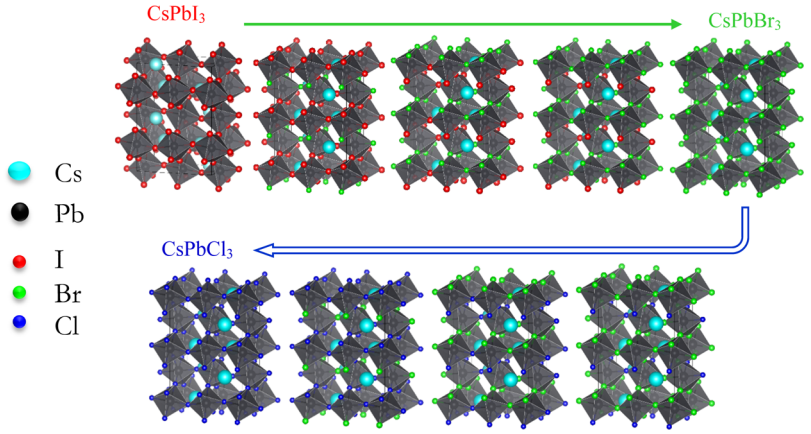

Figure 1. Crystal structure of mixed-halide inorganic perovskites.

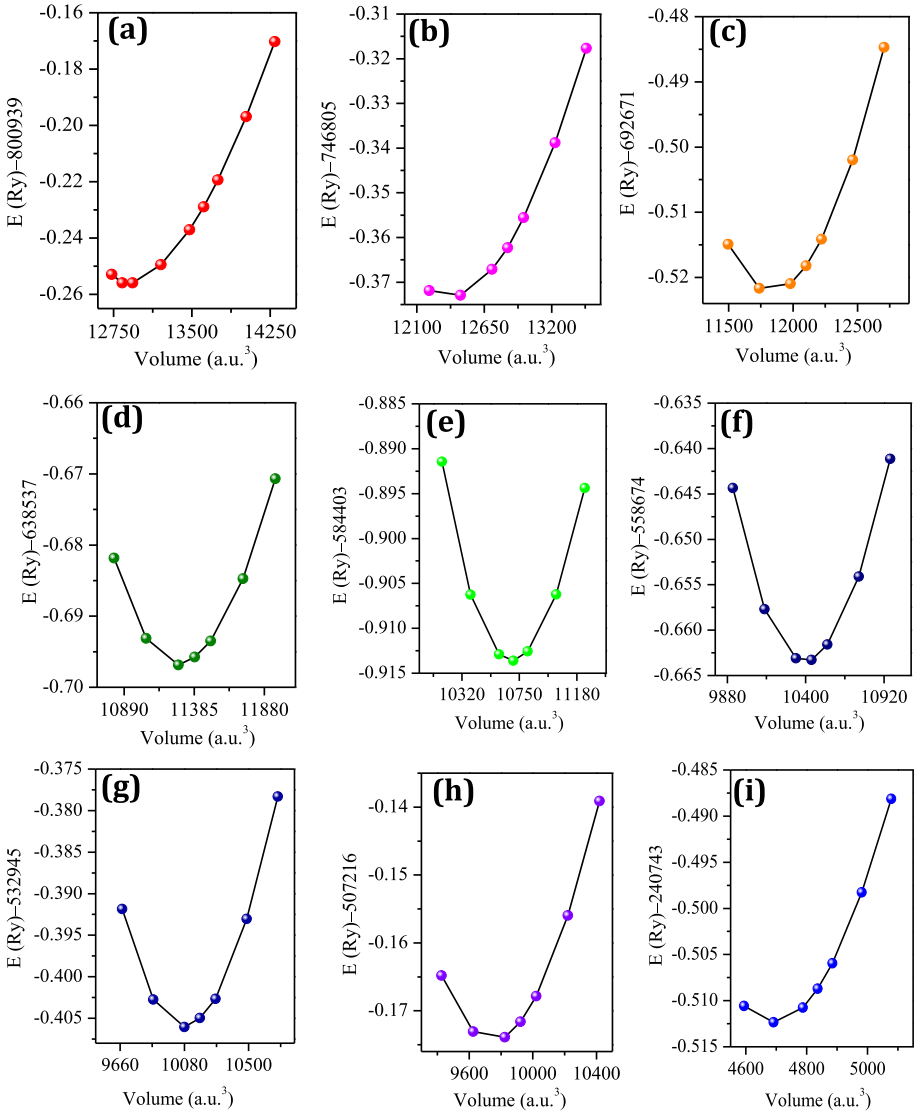

Figure 2. Variation in total energy with volume for (a) $CsPbI_3$, (b) $CsPbI_{2.25}Br_{0.75}$, (c) $CsPbI_{1.50}Br_{1.50}$. (d) $CsPbI_{0.75}Br_{2.25}$, (e) $CsPbBr_3$, (f) $CsPbBr_{2.25}Cl_{0.75}$, (g) $CsPbBr_{1.50}Cl_{1.50}$, (h) $CsPbBr_{0.75}Cl_{2.25}$, and (i) $CsPbCl_3$ obtained using the PBE-GGA potential.

Castelli et al. investigated the trends over band gaps for 240 perovskites composed of organic−inorganic cations, Sn and Pb as B-ion, and halides as anions.[23] The optoelectronic properties of mixed inorganic perovskites at the orthorhombic phase (*Pnma*) have not yet been investigated in detail, particularly the mixed halide from I to Br and Cl. It is advantageous to investigate the optoelectronic properties of mixed orthorhombic (*Pnma*) inorganic perovskites, which are available at room

https://doi.org/10.1021/acsomega.1c04806
ACS Omega 2021, 6, 30752−30761

Table 1. Theoretical Lattice Parameters (a, b, and c), Unit-Cell Volume V (Å)^3, Pressure Derivatives (B'), Bulk Modulus B (GPa), and Total Energy (E) for Mixed-Halide Perovskites. Note: The lattice Parameter, c has been doubled.

Mixed halide perovskites		a (Å)	b (Å)	c (Å)	V(Å)^3	B`	B (GPa)	Total energy E (Ry)
$CsPbI_3$	This work	8.93	12.76	17.71	2017.394	4.357	17.85	-800964.3712
	Previouse work	8.906[76] (8.8561)[78,82] (10.458)[79,83]	12.665[76] (8.577)[78,82] (4.802)[79,83]	8.198[76] (12.472)[78,82] (17.776)[79,83]				
$CsPbI_{2.25}Br_{0.75}$	This work	8.76	12.50	17.38	1903.098	5.448	19.52	-746912.3966
$CsPbI_{1.50}Br_{1.50}$		8.58	12.25	17.05	1793.199	5.441	20.10	-692776.4668
$CsPbI_{0.75}Br_{2.25}$		8.42	12.00	16.72	1687.614	6.096	21.35	-638692.1949
$CsPbBr_3$	This work	8.24	11.74	16.39	1586.254	5.799	22.65	-584536.6893
	Previouse work	8.244[16,68] (8.208)[63,80,81]	11.735[16,68] (11.763)[63,80,81]	8.1982[16,68] (8.257)[63,80,81]				
$CsPbBr_{2.25}Cl_{0.75}$	This work	8.18	11.64	16.25	1547.011	5.427	23.44	-558781.0674
$CsPbBr_{1.50}Cl_{1.50}$		8.03	11.63	15.87	1482.081	4.866	24.21	-533010.0061
$CsPbBr_{0.75}Cl_{2.25}$		8.02	11.45	15.77	1448.388	5.581	25.69	-507337.2300
$CsPbCl_3$	This work	7.97	11.36	15.83	1433.32	5..654	25.62	-481486.4912
	Previouse work	(7.976)[16,81]	(11.356)[16,81]	(7.9173)[16,81]				

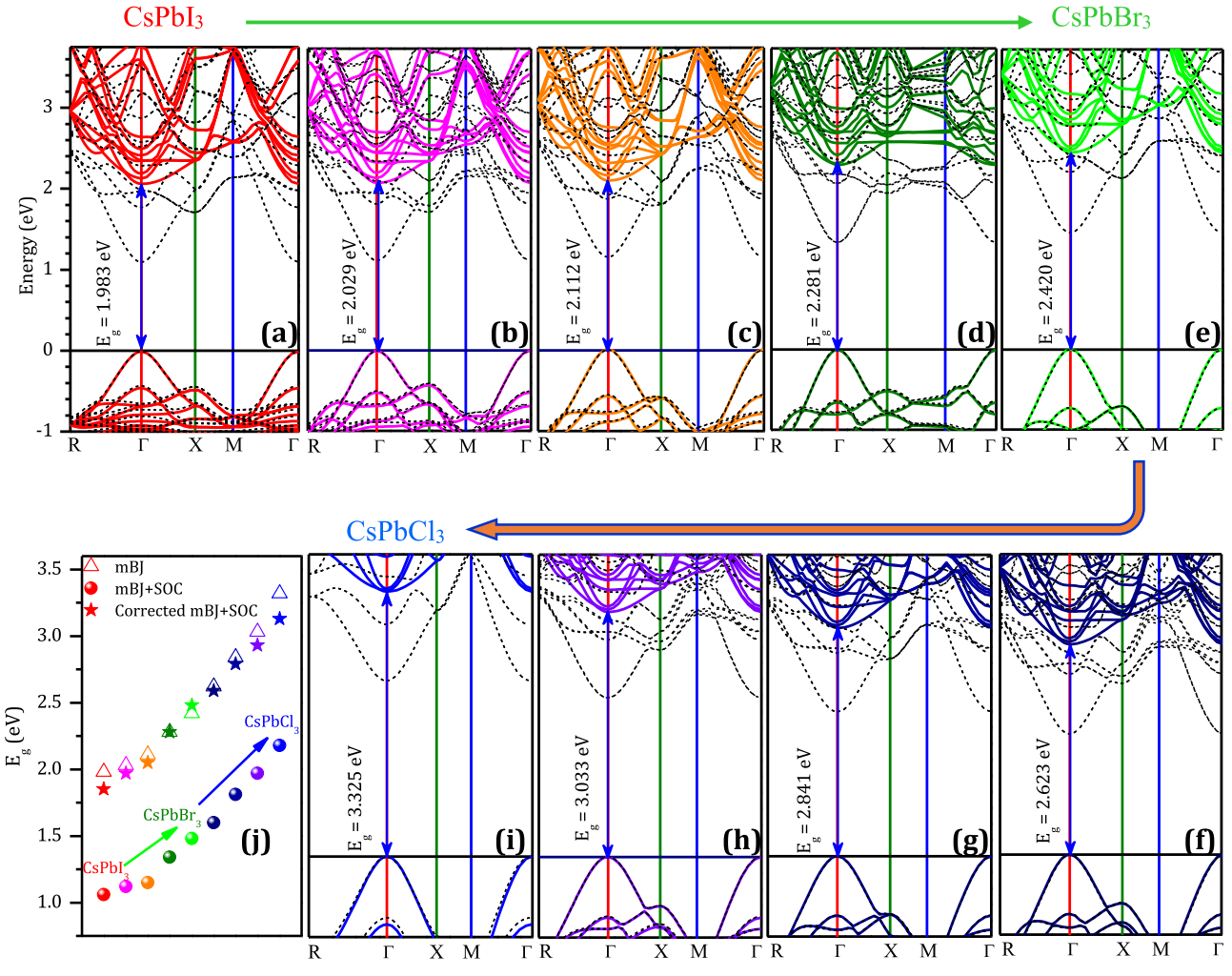

Figure 3. Band structure of (a) $CsPbI_3$, (b) $CsPbI_{2.25}Br_{0.75}$, (c) $CsPbI_{1.50}Br_{1.50}$, (d) $CsPbI_{0.75}Br_{2.25}$, (e) $CsPbBr_3$, (f) $CsPbBr_{2.25}Cl_{0.75}$, (g) $CsPbBr_{1.50}Cl_{1.50}$, (h) $CsPbBr_{0.75}Cl_{2.25}$, and (i) $CsPbCl_3$ obtained using mBJ-GGA potential without/with SOC. The band gap values versus the concentration of Br and then Cl calculated using mBJ, mBJ + SOC, and the corrected mBJ + SOC (j). The black dashed line represents the band structure calculated with mBJ + SOC. The VBM is set as zero.

temperature and have applications in solar cells, LEDs, and lasers, using the most accurate DFT calculation methods.

In this study, the mBJ-GGA method without/with spin orbital coupling (SOC)[47−50] was used to look into the impact of halide composition on the electronic and optical properties of mixed

https://doi.org/10.1021/acsomega.1c04806
ACS Omega 2021, 6, 30752−30761

orthorhombic perovskites 1 × 1 × 2 $CsPb(I_{1-x}Br_x)_3$ and $CsPb(Br_{1-x}Cl_x)_3$ (x = 0.00, 0.25, 0.50, 0.75, and 1.00), while the PBE-GGA method was used to investigate their structural properties. The mBJ-GGA method demonstrated the evolution of band structure, optical absorption, and energy band gap (E_g) with increasing x in $CsPb(I_{1-x}Br_x)_3$ and $CsPb(Br_{1-x}Cl_x)_3$. The lattice constants and E_g were computed and found to be consistent with previous research.[10,11,14,20,21,27,28,31,43,51−60] Furthermore, the effective masses of charge carriers, absorption, optical dielectric, and reflectivity were precisely calculated.

2. RESULTS AND DISCUSSION

2.1. Optimized Structures. At room temperature, $CsPbX_3$ (X = I, Br, Cl) perovskites have orthorhombic structures with space group *Pnma*.[17,61−71] Using VESTA software,[72] a supercell 1 × 1 × 2 with 40 atoms was used to simulate $CsPb(I_{1-x}Br_x)_3$ and $CsPb(Br_{1-x}Cl_x)_3$ perovskites. Starting with an orthorhombic inorganic $CsPbI_3$ structure, a supercell of $CsPb(I_{1-x}Br_x)_3$ and $CsPb(Br_{1-x}Cl_x)_3$ was created. The iodide was gradually replaced by an appropriate x concentration of Br, and Br was gradually replaced by an appropriate x concentration of Cl as shown in Figure 1. The structural properties of mixed-halide perovskites are investigated using first-principles DFT with the PBE-GGA method, which is implemented in the WIEN2k code.[33,73] The structural information is presented in Tables S1−S9, Supporting Information. Figure 2a−i shows the fitting of total energy as a function of volume using the Murnaghan equation of state[74] to compute the lattice constants of the perovskites. Table 1 displays the calculated lattice parameters (a, b, and c), unit-cell volume (V), pressure derivatives (B'), bulk modulus (B), and total energy (E) along with measured and previously predicted values for comparison. Our calculated data are roughly consistent with those measured and previously predicted values, indicating the reliability of the current computational scheme.[15,16,61,62,67,75−79] Figure S1 shows that as the concentration of Br and Cl increases, the volume of the unit-cell decreases.

3.2. Electronic Properties. The electronic properties of mixed-halide perovskites are investigated using the mBJ-GGA method without/with SOC, which is implemented in the WIEN2k code.[33,73] The electronic band structures without/with SOC follow the high-symmetry k-point path R → Γ → X → M → Γ as shown in Figure 3a−i. The SOC had a significant effect on the conduction band (CB) region, with a sharp reduction in the bottom of the CB,[47,82] whereas there was no significant change in the valence band (VB)[40] (see Supporting Information, Figure S2, SOC). The conduction band minimum (CBM) and valence band maximum (VBM) were found to be localized at the Γ point. Table 2 shows the E_g calculated with mBJ-GGA ranging from 1.983 eV for $CsPbI_3$ to 3.325 eV for $CsPbCl_3$, while E_g calculated with mBJ + SOC ranges from 1.066 eV for $CsPbI_3$ to 2.182 eV for $CsPbCl_3$, which is consistent with previous theoretical predictions.[15,16,75,79,80,83−87] Because of its proper band gap of 1.983 eV, $CsPbI_3$ is suitable for light-absorber applications, whereas $CsPbBr_3$ and $CsPbCl_3$ with band gaps of 2.420 and 3.325 eV, respectively, show promising application prospects in solar cells, LEDs, lasers, and photodetectors.[88] Because the E_g values with SOC are small in comparison to the experimental results, the alloy formula was used to correct the E_g determined by the mBJ-GGA + SOC method[14,89−92]

$$\Delta E_g(A_{1-x}B_x) = (1 - x)\Delta E_g(A) + x\Delta E_g(B) \quad (1)$$

Table 2. Band gap E_g (eV) Values for Mixed-Halide Inorganic Perovskites Compared With Previous Experimental and Theoretical Studies

	this work			
mixed-halide perovskites	mBJ	mBJ + SOC	corrected mBJ + SOC	other DFT(exp.)
$CsPbI_3$	1.983	1.066	1.850	1.831,[77,86] 1.48,[87] (1.75),[88] (1.85)[81]
$CsPbI_{2.25}Br_{0.75}$	2.029	1.123	2.064	(2.010)[81]
$CsPbI_{1.50}Br_{1.50}$	2.112	1.151	2.079	1.93,[86] (1.97),[76] (2.17)[81]
$CsPbI_{0.75}Br_{2.25}$	2.281	1.343	2.276	(2.17),[88] (2.23)[81]
$CsPbBr_3$	2.420	1.482	2.480	2.32,[90] 2.40,[86] (2.38),[94] (2.479)[81]
$CsPbBr_{2.25}Cl_{0.75}$	2.623	1.602	2.593	(2.670)[81]
$CsPbBr_{1.50}Cl_{1.50}$	2.841	1.815	2.791	(2.720),[76] (2.800)[81]
$CsPbBr_{0.75}Cl_{2.25}$	3.033	1.973	2.933	(2.940)[81]
$CsPbCl_3$	3.325	2.182	3.130	3.05,[10] (2.91),[16] (2.78),[95] (3.132)[81]

where $\Delta E_g(A_{1-x}B_x)$ is the change in band gap for the mixed $CsPb(I_{1-x}Br_x)_3$ and $CsPb(Br_{1-x}Cl_x)_3$ perovskites, $\Delta E_g(A)$ is the change in band gap for pure $CsPbI_3$/$CsPbBr_3$, and $\Delta E_g(B)$ is the change in band gap for pure $CsPbBr_3$/$CsPbCl_3$. Table 2 shows that the corrected mBJ-GGA + SOC E_g ranges from 1.850 eV for $CsPbI_3$ to 3.130 eV for $CsPbCl_3$. Figure 3j shows the dramatic increase in E_g caused by replacing I with Br, followed by Cl. Electron (m_e^*) and hole (m_h^*) effective masses are important indicators of photovoltaic material transport properties.[10] Lead, halides, and the symmetries of the perovskite structure all play important roles in determining the effective mass of electrons and holes. The CBM band edges were significantly flatter than the VBM, indicating that electrons had far more mass than holes.[60] The effective masses, m_e^* and m_h^*, were calculated using the equation $(m^*)_{ij} = \hbar^2\left[\frac{\partial^2\varepsilon_n(\vec{k})}{\partial k_i k_j}\right]^{-1}$ where m^* is the effective mass of the electron or hole, i and j denote the reciprocal components, $\varepsilon_n(k\rightharpoonup)$ is the energy dispersion function of the nth band, and $k\rightharpoonup$ represents the wave vector. The effective masses, m_e^* and m_h^*, without SOC ranged from 0.13579 to 0.23119m_0 and from 0.07099 to 0.09354m_0, respectively, and those with SOC ranged from 0.06019 to 0.08938m_0 and from 0.06828 to 0.08354m_0, respectively. As indicated by Figure 4, the calculated reduced effective mass[82] $\mu = \frac{m_e^* m_h^*}{m_e^* + m_h^*}$ without/with SOC increased significantly with increasing Br and Cl concentration in $CsPb(I_{1-x}Br_x)_3$ and $CsPb(Br_{1-x}Cl_x)_3$ respectively. Table S10 in the Supporting Information contains additional information on the effective mass of the electron and hole and the reduced mass (μ) for mixed-halide perovskites.

3.3. Density of States. Figure 5 shows that the total density of states (TDOS) remained unchanged as the concentration (x) increased from 0.00 to 1.00 of Br and Cl in $CsPb(I_{1-x}Br_x)_3$ and $CsPb(Br_{1-x}Cl_x)_3$ perovskites, but the edges were shifted up, where the VBM was shifted to 0 eV. The partial DOS (PDOS) for the mixed perovskite demonstrates that Cs^+ has no effect on the VBM or CBM but only maintains overall load neutrality and structural stability[11,14,28,40,76,93−97] as shown in Figure S3, Supporting Information. The VBM is primarily derived from the p orbitals of I, Br, and Cl, with contributions from the s

https://doi.org/10.1021/acsomega.1c04806
ACS Omega 2021, 6, 30752−30761

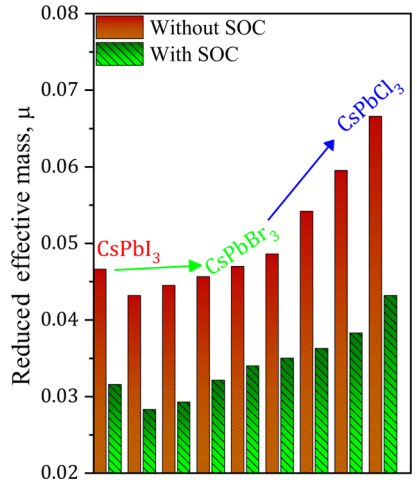

Figure 4. Reduced effective masses μ for mixed inorganic perovskites.

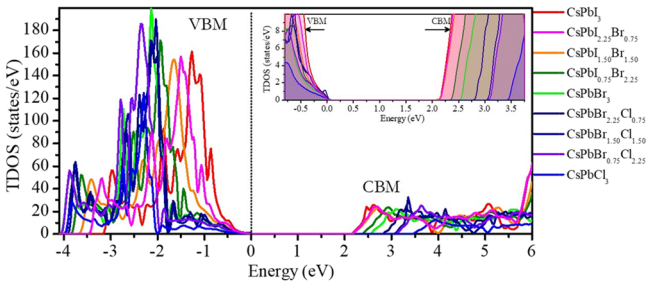

Figure 5. TDOS of mixed-inorganic perovskites. Inset: TDOS in the range −0.8 to 3.75 eV.

orbitals of Pb. The CBM was formed mostly by the p states of Pb and minor contribution by the s and p states of I, Cl, and Br. An in-depth look at the band structure of $CsPbI_3$, $CsPbI_{1.50}Br_{1.50}$, $CsPbBr_3$, $CsPbBr_{1.50}Cl_{1.50}$, and $CsPbCl_3$ with respect to PDOS is shown in Figure S4, Supporting Information.

3.4. Electron Density. To visualize the charge distribution and bonding nature of $CsPbI_3$, $CsPbI_{2.25}Br_{0.75}$, $CsPbI_{1.50}Br_{1.50}$, $CsPbI_{0.75}Br_{2.25}$, $CsPbBr_3$, $CsPbBr_{2.25}Cl_{0.75}$, $CsPbBr_{1.50}Cl_{1.50}$, $CsPbBr_{0.75}Cl_{2.25}$, and $CsPbCl_3$ perovskites, the electron density distribution is investigated and presented in Figure 6. The atoms Cs, Pb, I, Br, and Cl have electronegativity values of 0.79, 2.33, 2.66, 2.96, and 3.16 on the Pauling scale, respectively. The difference in electronegativity $(X_1 - X_2)$ is critical for describing the bonding character.[98] The following equation is used to calculate the percentage of ionic character (IC) of the bonding obtained[31,98,99]

$$\% \text{ IC} = [1 - e^{-(0.25)(X_1 - X_2)^2}] \times 100 \quad (2)$$

The electronegativities of the 1 and 2 atoms are represented by X_1 and X_2, respectively. The % IC of Cs−Br, Cs−I, and Cs−Cl was 69.18, 58.28, and 75.44, whereas for Pb−Br, Pb−I, and Pb−Cl, was 9.45, 2.69, and 15.82, respectively. The electron clouds surrounding Cs atoms are spherical and free of distortion, indicating that they are mostly ionic and partially covalent with the surrounding atoms.[21,31,100] In contrast, the bond between Pb and I, Br, or Cl is mostly covalent and partially ionic, with electron clouds around these atoms distorted and overlapping significantly.

3.5. Optical Properties. We investigate the optical properties of mixed-halide perovskites, including dielectric function, refractive index, extinction coefficient, reflectivity,

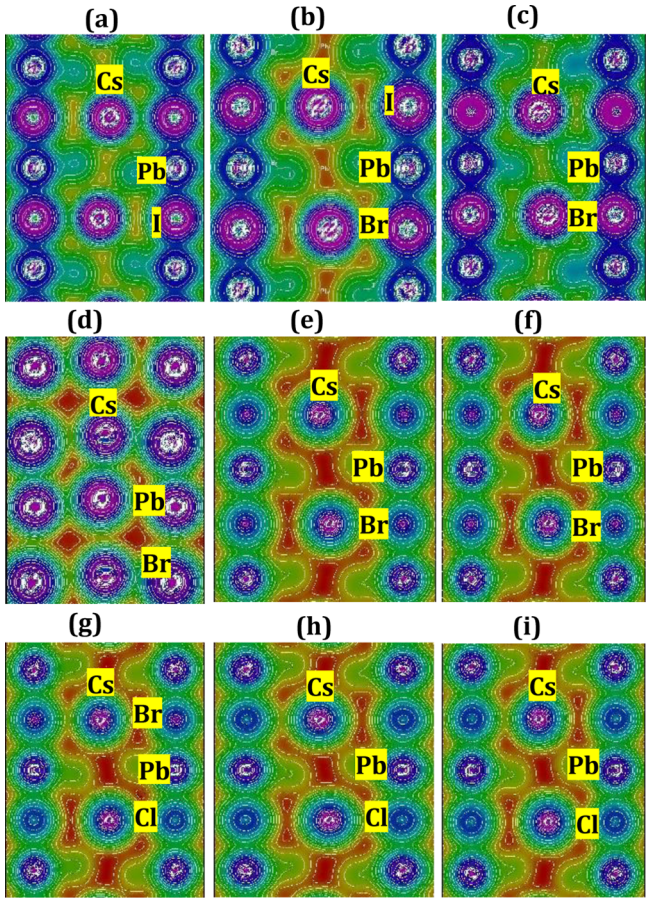

Figure 6. Calculated electron density distribution of (a) $CsPbI_3$, (b) $CsPbI_{2.25}Br_{0.75}$, (c) $CsPbI_{1.50}Br_{1.50}$, (d) $CsPbI_{0.75}Br_{2.25}$, (e) $CsPbBr_3$, (f) $CsPbBr_{2.25}Cl_{0.75}$, (g) $CsPbBr_{1.50}Cl_{1.50}$, (h) $CsPbBr_{0.75}Cl_{2.25}$, and (i) $CsPbCl_3$.

and optical absorption for energy ranging from 0 to 10 eV. The calculated dielectric functions $\varepsilon_1(\omega)$ and $\varepsilon_2(\omega)$ are shown in Figure 7a,b. The dielectric function describes how a material responds to incident photons as a function of energy. The real part of the dielectric function $\varepsilon_1(\omega)$ value at zero frequency is known as the static frequency $\varepsilon_1(0)$, and it varies between 4.72 and 3.12 as shown in Figure 8. Figure 7b shows the behavior of the imaginary part of the dielectric function $\varepsilon_2(\omega)$, where it represents the radiation absorbed by the compound,[31,101] with main peaks between 3.42 and 6.68 eV. It is worth noting that $\varepsilon_2(\omega)$ has a zero value until absorption begins after the photon energy reaches the band gap energy, which establishes the threshold for a direct optical transition between the VBM and the CBM.

The refractive index $n(\omega)$ and extinction coefficient $k(\omega)$ were calculated, as shown in Figure S5a,b, Supporting Information. $n(\omega)$ is a critical feature of semiconductors that indicates how much light is bent or refracted.[101] The value of $n(\omega)$ increases as the energy increases up to 2.87 and 2.14 for $CsPbI_3$ and $CsPbCl_3$, and then it begins to decrease to 1.27 and 1.44 showing a nonlinear behavior as shown in Figure S5a. For $CsPbI_3$, $CsPbBr_3$, and $CsPbCl_3$, the calculated $n(0)$ values were 2.17, 1.95, and 1.77 which agree well with the previous theoretical and experimental values[31,55,102] as shown in Figure 8. Figure S5b shows that $k(\omega)$ is proportional to Br/Cl concentration, similar to $\varepsilon_2(\omega)$, with the local maximum

https://doi.org/10.1021/acsomega.1c04806
ACS Omega 2021, 6, 30752−30761

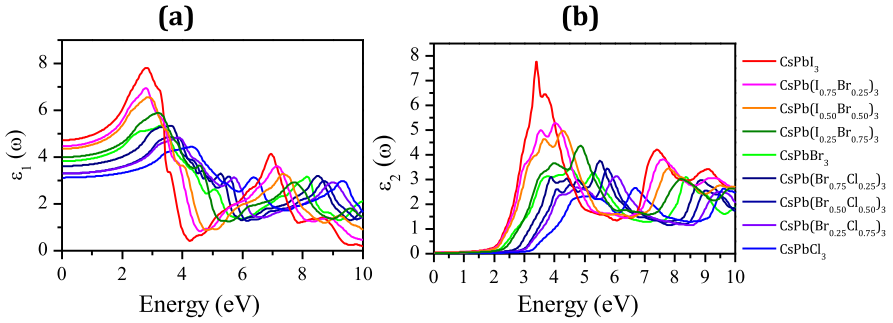

Figure 7. (a) Real dielectric function $\varepsilon_1(\omega)$ and (b) imaginary dielectric function $\varepsilon_2(\omega)$ of mixed-halide perovskites.

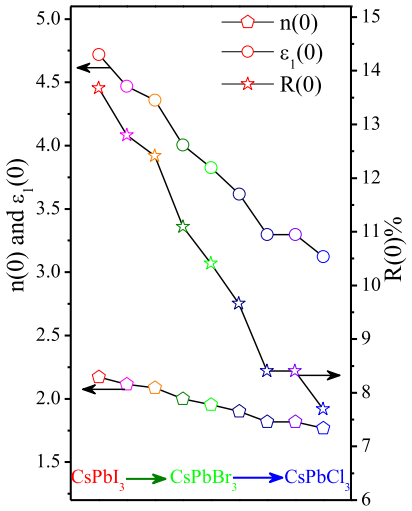

Figure 8. Static dielectric constant $\varepsilon_1(0)$, refractive index $n(0)$, and reflectivity $R(0)$% of mixed-halide perovskites with different dopant concentrations x.

occurring between 3.89 and 6.72 eV when moving from $CsPbI_3$ to $CsPbCl_3$.

The calculated reflectivity $R(\omega)$ in relation to incident energy is shown in Figure S6, Supporting Information. The mixed perovskites behaved as semiconductors; the value of $R(\omega)$ was not unity at zero energy.[103] At zero frequency, $CsPbI_3$ has a static reflectivity $R(0)$ value of 13.7%, which then decreases to 10.4 and 7.7% for $CsPbBr_3$ and $CsPbCl_3$, respectively. When moving from $CsPbI_3$ to $CsPbBr_3$ and $CsPbCl_3$, the maximum $R(\omega)$ occurs between 3.22 and 4.71 eV, and it begins to fluctuate and decrease at higher energies. As shown in Figure 8, the calculated $R(0)$ at zero energy was approximately 13.65, 12.78, 12.42, 11.01, 10.43, 9.66, 8.42, 8.33, and 7.67% for mixed perovskite when transitioning from $CsPbI_3$ to $CsPbBr_3$ and $CsPbCl_3$.

Figure 9a exhibits the absorption coefficient, $\alpha(\omega)$, as a function of the energy. $\alpha(\omega)$ peaks shifted to higher energies with increasing Br and Cl concentrations in $CsPb(I_{1-x}Br_x)_3$ and $CsPb(Br_{1-x}Cl_x)_3$. The wide absorption coefficient range from visible to ultraviolet indicates that they are useful for a variety of optical and optoelectronic applications.[31] Figure 9b shows the optical conductivity $\sigma(\omega)$ characteristics, which are analogous to $\alpha(\omega)$ and provide information on how external parameters affect the electronic structure. The optical properties of the studied perovskite were consistent with those previously measured and reported.[11,31]

3. CONCLUSIONS

In this study, the influence of halide composition on the optoelectronic properties of mixed-halide perovskites was investigated. The structural properties were calculated using the PBE-GGA method, and the lattice parameters are well comparable to previous experimental and theoretical work. When iodide (I) was replaced with bromide (Br) and then chloride (Cl), the unit-cell volume decreased linearly. The calculated band gap (E_g) using the mBJ-GGA method is in good agreement with the experimental values reported, and it increased clearly from 1.983 eV for $CsPbI_3$ to 2.420 and 3.325 eV for $CsPbBr_3$ and $CsPbCl_3$, respectively, due to the increase in electronegativity of Br and Cl. Because the E_g values with mBJ + SOC are small compared to the experimental results, the alloy formula was used to correct the E_g values. The corrected mBJ + SOC E_g value is 1.850 eV for $CsPbI_3$ and 2.480 and 3.130 eV for $CsPbBr_3$ and $CsPbCl_3$, respectively. The reduced masses (μ) are correlated with the energies of E_g, VBM, and CBM. When moving from $CsPbI_3$ to $CsPbBr_3$ and $CsPbCl_3$, μ ranges from $0.046618m_o$ to $0.066595m_o$ without SOC and from $0.031569m_o$ to $0.043181m_o$ with SOC. As the Br and Cl content increases, the calculated photoabsorption coefficients show a blue shift in

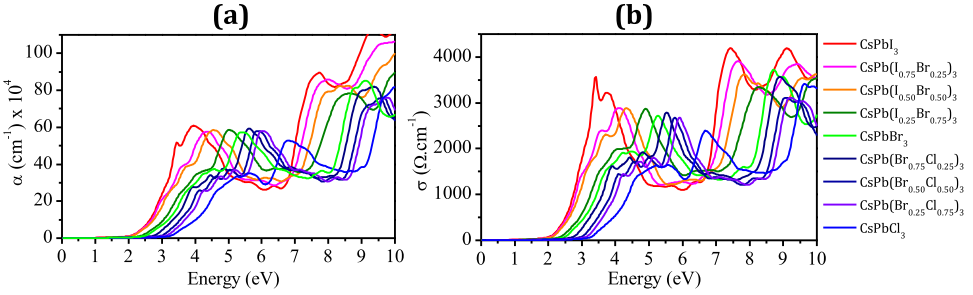

Figure 9. (a) Calculated absorption spectra $\alpha(\omega)$ and (b) conductivity $\sigma(\omega)$ of mixed-halide perovskites with different dopant concentrations x.

https://doi.org/10.1021/acsomega.1c04806
ACS Omega 2021, 6, 30752−30761

the absorption coefficient. According to the calculations, these perovskites can be used in solar cells, LEDs, and laser applications.

3.1. Computational Method. The FP-LAPW method within the framework of DFT as implemented in the WIEN2k code was used to optimize the structure of the mixed inorganic perovskites.[33,73] The PBE-GGA method was used to calculate the structural properties of the mixed perovskites. The mixed inorganic perovskite structures were created by building a 1 × 1 × 2 supercell with a binary perovskite's *Pnma* space group. Because of the presence of a heavy element (Pb) in the structure, the SOC interaction[47−50,104,105] was used with mBJ-GGA, as described in our previous work.[40] To match the experimental values, the calculated band gap with SOC was corrected by using the alloy formula.[14,89,90] During the calculation, $RK_{max} = 9$ and *k*-points = 100 were used, and the total energy was converged to 10^{-4} Ry.

■ ASSOCIATED CONTENT

Supporting Information

The Supporting Information is available free of charge at https://pubs.acs.org/doi/10.1021/acsomega.1c04806.

Structural parameters; unit-cell volume versus Br and Cl contents; SOC; energy level splitting diagram for the orthorhombic phase of inorganic perovskites; PDOS of mixed inorganic perovskites; band structures; calculated effective mass of the electron and hole and reduced mass for mixed-halide perovskites; and calculated refraction indices and extinction coefficients and reflectivity spectra of mixed-halide perovskites with different dopant concentrations (PDF)

■ AUTHOR INFORMATION

Corresponding Authors

Hamid M. Ghaithan − *Physics and Astronomy Department, College of Science, King Saud University, Riyadh 11451, Saudi Arabia;* orcid.org/0000-0001-5126-4477; Phone: +966 532257491; Email: hghaithan@ksu.edu.sa

Zeyad. A. Alahmed − *Physics and Astronomy Department, College of Science, King Saud University, Riyadh 11451, Saudi Arabia*; Email: zalahmed@ksu.edu.sa

Abdullah S. Aldwayyan − *Physics and Astronomy Department, College of Science and King Abdullah Institute for Nanotechnology, King Saud University, Riyadh 11451, Saudi Arabia; K.A.CARE Energy Research and Innovation Center at Riyadh, Riyadh 11454, Saudi Arabia*; Email: dwayyan@ksu.edu.sa

Author

Saif M. H. Qaid − *Physics and Astronomy Department, College of Science, King Saud University, Riyadh 11451, Saudi Arabia;* orcid.org/0000-0001-8958-8960

Complete contact information is available at: https://pubs.acs.org/10.1021/acsomega.1c04806

Notes

The authors declare no competing financial interest.

■ ACKNOWLEDGMENTS

The authors thank the Deanship of Scientific Research at King Saud University for funding this work through Research Group No. RG-1440-038.

■ REFERENCES

(1) Xiang, W.; Tress, W. Review on Recent Progress of All-Inorganic Metal Halide Perovskites and Solar Cells. *Adv. Mater.* **2019**, *31*, 1902851.

(2) Dang, Y.; Ju, D.; Wang, L.; Tao, X. Recent Progress in the Synthesis of Hybrid Halide Perovskite Single Crystals. *CrystEngComm* **2016**, *18*, 4476−4484.

(3) Wang, B.; Xiao, X.; Chen, T. Perovskite Photovoltaics: A High-Efficiency Newcomer to the Solar Cell Family. *Nanoscale* **2014**, *6*, 12287−12297.

(4) Jong, U.-G.; Yu, C.-J.; Kim, Y.-S.; Kye, Y.-H.; Kim, C.-H. First-Principles Study on the Material Properties of the Inorganic Perovskite $Rb_{1-x}Cs_xPbI_3$ for Solar Cell Applications. *Phys. Rev. B: Condens. Matter Mater. Phys.* **2018**, *98*, 125116.

(5) Zhang, L.; Yang, X.; Jiang, Q.; Wang, P.; Yin, Z.; Zhang, X.; Tan, H.; Yang, Y. M.; Wei, M.; Sutherland, B. R.; et al. Ultra-Bright and Highly Efficient Inorganic Based Perovskite Light-Emitting Diodes. *Nat. Commun.* **2017**, *8*, 15640.

(6) Veldhuis, S. A.; Boix, P. P.; Yantara, N.; Li, M.; Sum, T. C.; Mathews, N.; Mhaisalkar, S. G. Perovskite Materials for Light-Emitting Diodes and Lasers. *Adv. Mater.* **2016**, *28*, 6804−6834.

(7) Song, J.; Li, J.; Li, X.; Xu, L.; Dong, Y.; Zeng, H. Quantum Dot Light-Emitting Diodes Based on Inorganic Perovskite Cesium Lead Halides ($CsPbX_3$). *Adv. Mater.* **2015**, *27*, 7162−7167.

(8) Xing, J.; Yan, F.; Zhao, Y.; Chen, S.; Yu, H.; Zhang, Q.; Zeng, R.; Demir, H. V.; Sun, X.; Huan, A.; et al. High-Efficiency Light-Emitting Diodes of Organometal Halide Perovskite Amorphous Nanoparticles. *ACS Nano* **2016**, *10*, 6623−6630.

(9) Li, X.; Cao, F.; Yu, D.; Chen, J.; Sun, Z.; Shen, Y.; Zhu, Y.; Wang, L.; Wei, Y.; Wu, Y.; et al. All Inorganic Halide Perovskites Nanosystem: Synthesis, Structural Features, Optical Properties and Optoelectronic Applications. *Small* **2017**, *13*, 1603996.

(10) Mao, X.; Sun, L.; Wu, T.; Chu, T.; Deng, W.; Han, K. First-Principles Screening of All-Inorganic Lead-Free ABX_3 Perovskites. *J. Phys. Chem. C* **2018**, *122*, 7670−7675.

(11) Ahmad, M.; Rehman, G.; Ali, L.; Shafiq, M.; Iqbal, R.; Ahmad, R.; Khan, T.; Jalali-Asadabadi, S.; Maqbool, M.; Ahmad, I. Structural, Electronic and Optical Properties of $CsPbX_3$ (X=Cl, Br, I) for Energy Storage and Hybrid Solar Cell Applications. *J. Alloys Compd.* **2017**, *705*, 828−839.

(12) Filip, M. R.; Eperon, G. E.; Snaith, H. J.; Giustino, F. Steric Engineering of Metal-Halide Perovskites with Tunable Optical Band Gaps. *Nat. Commun.* **2014**, *5*, 5757.

(13) Fang, Z.; Shang, M.; Hou, X.; Zheng, Y.; Du, Z.; Yang, Z.; Chou, K.-C.; Yang, W.; Wang, Z. L.; Yang, Y. Bandgap Alignment of α-$CsPbI_3$ Perovskites with Synergistically Enhanced Stability and Optical Performance via B-Site Minor Doping. *Nano Energy* **2019**, *61*, 389−396.

(14) Chen, X.; Han, D.; Su, Y.; Zeng, Q.; Liu, L.; Shen, D. Structural and Electronic Properties of Inorganic Mixed Halide Perovskites. *Phys. Status Solidi Rapid Res. Lett.* **2018**, *12*, 1800193.

(15) Ray, D.; Clark, C.; Pham, H. Q.; Borycz, J.; Holmes, R. J.; Aydil, E. S.; Gagliardi, L. Computational Study of Structural and Electronic Properties of Lead-Free $CsMI_3$ Perovskites (M = Ge, Sn, Pb, Mg, Ca, Sr, and Ba). *J. Phys. Chem. C* **2018**, *122*, 7838−7848.

(16) Linaburg, M. R.; McClure, E. T.; Majher, J. D.; Woodward, P. M. $Cs_{1-x}Rb_xPbCl_3$ and $Cs_{1-x}Rb_xPbBr_3$ Solid Solutions: Understanding Octahedral Tilting in Lead Halide Perovskites. *Chem. Mater.* **2017**, *29*, 3507−3514.

(17) Dos Reis, R.; Yang, H.; Ophus, C.; Ercius, P.; Bizarri, G.; Perrodin, D.; Shalapska, T.; Bourret, E.; Ciston, J.; Dahmen, U. Determination of the Structural Phase and Octahedral Rotation Angle in Halide Perovskites. *Appl. Phys. Lett.* **2018**, *112*, 071901.

(18) Arkan, F.; Izadyar, M. Computational Modeling of the Photovoltaic Activities in $EABX_3$ (EA = Ethylammonium, B = Pb, Sn, Ge, X = Cl, Br, I) Perovskite Solar Cells. *Comput. Mater. Sci.* **2018**, *152*, 324−330.

(19) Wang, Y.; Gould, T.; Dobson, J. F.; Zhang, H.; Yang, H.; Yao, X.; Zhao, H. Density Functional Theory Analysis of Structural and

Electronic Properties of Orthorhombic Perovskite $CH_3NH_3PbI_3$. *Phys. Chem. Chem. Phys.* **2014**, *16*, 1424−1429.
(20) Qian, J.; Xu, B.; Tian, W. A Comprehensive Theoretical Study of Halide Perovskites ABX_3. *Org. Electron Phys. Mater. Appl.* **2016**, *37*, 61−73.
(21) Lang, L.; Yang, J.-H.; Liu, H.-R.; Xiang, H. J.; Gong, X. G. First-Principles Study on the Electronic and Optical Properties of Cubic ABX_3 Halide Perovskites. *Phys. Lett. A* **2014**, *378*, 290−293.
(22) Dastidar, S.; Egger, D. A.; Tan, L. Z.; Cromer, S. B.; Dillon, A. D.; Liu, S.; Kronik, L.; Rappe, A. M.; Fafarman, A. T. High Chloride Doping Levels Stabilize the Perovskite Phase of Cesium Lead Iodide. *Nano Lett.* **2016**, *16*, 3563−3570.
(23) Castelli, I. E.; García-Lastra, J. M.; Thygesen, K. S.; Jacobsen, K. W. Bandgap Calculations and Trends of Organometal Halide Perovskites. *APL Mater.* **2014**, *2*, 081514.
(24) Giorgi, G.; Fujisawa, J.-I.; Segawa, H.; Yamashita, K. Cation Role in Structural and Electronic Properties of 3D Organic-Inorganic Halide Perovskites. A DFT Analysis. *J. Phys. Chem. C* **2014**, *118*, 12176−12183.
(25) Fang, Z.; Yi, Z. First Principles Study on Mixed Orthorhombic Perovskite CH3NH3Pb$(I_{1-X}Br_x)_3$. *Chem. Phys. Lett.* **2017**, *687*, 19−22.
(26) Yang, R. X.; Skelton, J. M.; Da Silva, E. L.; Frost, J. M.; Walsh, A. Spontaneous Octahedral Tilting in the Cubic Inorganic Cesium Halide Perovskites CsSnX3 and $CsPbX_3$ (X = F, Cl, Br, I). *J. Phys. Chem. Lett.* **2017**, *8*, 4720−4726.
(27) Goesten, M. G.; Hoffmann, R. Mirrors of Bonding in Metal Halide Perovskites. *J. Am. Chem. Soc.* **2018**, *140*, 12996−13010.
(28) Jishi, R. A.; Ta, O. B.; Sharif, A. A. Modeling of Lead Halide Perovskites for Photovoltaic Applications. *J. Phys. Chem. C* **2014**, *118*, 28344−28349.
(29) Filip, M. R.; Giustino, F. Computational Screening of Homovalent Lead Substitution in Organic-Inorganic Halide Perovskites. *J. Phys. Chem. C* **2016**, *120*, 166−173.
(30) Bechtel, J. S.; Van Der Ven, A. First-Principles Thermodynamics Study of Phase Stability in Inorganic Halide Perovskite Solid Solutions. *Phys. Rev. Mater.* **2018**, *2*, 045401.
(31) Murtaza, G.; Ahmad, I. First Principle Study of the Structural and Optoelectronic Properties of Cubic Perovskites $CsPbM_3$ (M=Cl, Br, I). *Phys. Rev. B: Condens. Matter Mater. Phys.* **2011**, *406*, 3222−3229.
(32) Afsari, M.; Boochani, A.; Hantezadeh, M. Electronic, Optical and Elastic Properties of Cubic Perovskite $CsPbI_3$: Using First Principles Study. *Optik* **2016**, *127*, 11433−11443.
(33) Kohn, W.; Sham, S. A. L. J. Self-Consistent Equations Including Exchange and Correlation Effects. *Phys. Rev.* **1965**, *140*, A1133.
(34) Perdew, J. P.; Burke, K.; Ernzerhof, M. Generalized Gradient Approximation Made Simple. *Phys. Rev. Lett.* **1996**, *77*, 3865−3868.
(35) Ziesche, P.; Kurth, S.; Perdew, J. P. Density Functionals from LDA to GGA. *Comput. Mater. Sci.* **1998**, *11*, 122−127.
(36) Prudhvi Raju, N.; Thangavel, R. Theoretical Investigation of Spin−Orbit Coupling on Structural, Electronic and Optical Properties for $CuAB_2$ (A = Sb, Bi; B = S, Se) Compounds Using Tran−Blaha-Modified Becke−Johnson Method: A First-Principles Approach. *J. Alloys Compd.* **2020**, *830*, 154621.
(37) Tran, F.; Blaha, P. Implementation of Screened Hybrid Functionals Based on the Yukawa Potential within the LAPW Basis Set. *Phys. Rev. B: Condens. Matter Mater. Phys.* **2011**, *83*, 235118.
(38) Staroverov, V. N.; Scuseria, G. E.; Tao, J.; Perdew, J. P. Tests of a Ladder of Density Functionals for Bulk Solids and Surfaces. *Phys. Rev. B: Condens. Matter Mater. Phys.* **2004**, *69*, 075102.
(39) Kurth, S.; Perdew, J. P.; Blaha, P. Molecular and Solid-State Tests of Density Functional Approximations: LSD, GGAs, and Meta-GGAs. *Int. J. Quantum Chem.* **1999**, *75*, 889−909.
(40) Ghaithan, H. M.; Alahmed, Z. A.; Qaid, S. M. H.; Hezam, M.; Aldwayyan, A. S. Density Functional Study of Cubic, Tetragonal, and Orthorhombic $CsPbBr_3$ Perovskite. *ACS Omega* **2020**, *5*, 7468−7480.
(41) Camargo-Martínez, J. A.; Baquero, R. The Band Gap Problem: The Accuracy of the Wien2k Code Confronted. *Rev. Mex. Fis.* **2012**, *59*, 453−459.
(42) Tran, F.; Blaha, P. Importance of the Kinetic Energy Density for Band Gap Calculations in Solids with Density Functional Theory. *J. Phys. Chem. A* **2017**, *121*, 3318−3325.
(43) Ghaithan, H. M.; Alahmed, Z. A.; Qaid, S. M. H.; Aldwayyan, A. S. First Principle-Based Calculations of the Optoelectronic Features of 2 x 2 x 2 $CsPb(I_{1-X}Br_x)_3$ Perovskite. *Superlattices Microstruct.* **2020**, *140*, 106474.
(44) Koliogiorgos, A.; Garoufalis, C. S.; Galanakis, I.; Baskoutas, S. Electronic and Optical Properties of Ultrasmall ABX_3 (A = Cs, CH_3NH_3/B = Ge, Pb, Sn, Ca, Sr/X = Cl, Br, I) Perovskite Quantum Dots. *ACS Omega* **2018**, *3*, 18917−18924.
(45) Chen, X.; Han, D.; Su, Y.; Zeng, Q.; Liu, L.; Shen, D. Structural and Electronic Properties of Inorganic Mixed Halide Perovskites. *Phys. Status Solidi Rapid Res. Lett.* **2018**, *12*, 1800193.
(46) Saleev, V. A.; Shipilova, A. V. Ab Initio Modeling of Band Gaps of Cesium Lead Halide Perovskites Depending on the Dopant Amount. *J. Phys. Conf.* **2018**, *1096*, 012115.
(47) Afsari, M.; Boochani, A.; Hantezadeh, M.; Elahi, S. M. Topological Nature in Cubic Phase of Perovskite $CsPbI_3$: By DFT. *Solid State Commun.* **2017**, *259*, 10−15.
(48) Zhang, Q.; Su, R.; Du, W.; Liu, X.; Zhao, L.; Ha, S. T.; Xiong, Q. Advances in Small Perovskite-Based Lasers. *Small Methods* **2017**, *1*, 1700163.
(49) Even, J.; Pedesseau, L.; Jancu, J.-M.; Katan, C. Importance of Spin-Orbit Coupling in Hybrid Organic/Inorganic Perovskites for Photovoltaic Applications. *J. Phys. Chem. Lett.* **2013**, *4*, 2999−3005.
(50) Wang, K.; Yang, Q.; Duan, J.; Zhang, C.; Zhao, F.; Yu, H.; Hu, B. Spin-Polarized Electronic Transport through Ferromagnet/Organic−Inorganic Hybrid Perovskite Spinterfaces at Room Temperature. *Adv. Mater. Interfaces* **2019**, *6*, 1900718.
(51) Li, Y.; Duan, J.; He, B.; Tang, Q.; Zhao, Y.; Yuan, H. Lattice Modulation of Alkali Metal Cations Doped $Cs1_{-X}R_XPbBr_3$ Halides for Inorganic Perovskite Solar Cells. *Sol. RRL* **2018**, *2*, 1800164.
(52) Qaid, S. M. H.; Al-Asbahi, B. A.; Ghaithan, H. M.; AlSalhi, M. S.; Al dwayyan, A. S. Optical and Structural Properties of $CsPbBr_3$ Perovskite Quantum Dots/PFO Polymer Composite Thin Films. *J. Colloid Interface Sci.* **2020**, *563*, 426−434.
(53) Heidrich, K.; Schäfer, W.; Schreiber, M.; Söchtig, J.; Trendel, G.; Treusch, J.; Grandke, T.; Stolz, H. J. Electronic Structure, Photoemission Spectra, and Vacuum-Ultraviolet Optical Spectra of $CsPbCl_3$ and $CsPbBr_3$. *Phys. Rev. B: Condens. Matter Mater. Phys.* **1981**, *24*, 5642−5649.
(54) Pandey, N.; Kumar, A.; Chakrabarti, S. Investigation of the Structural, Electronic, and Optical Properties of Mn-Doped $CsPbCl_3$: Theory and Experiment. *RSC Adv.* **2019**, *9*, 29556−29565.
(55) Yakunin, S.; Protesescu, L.; Krieg, F.; Bodnarchuk, M. I.; Nedelcu, G.; Humer, M.; Luca, G. D.; Fiebig, M.; Heiss, W.; Kovalenko, M. V. Low-Threshold Amplified Spontaneous Emission and Lasing from Colloidal Nanocrystals of Caesium Lead Halide Perovskites Lead Halide Perovskites. *Nat. Commun.* **2015**, *6*, 8056.
(56) Yuan, Y.; Xu, R.; Xu, H. T.; Hong, F.; Xu, F.; Wang, L. J. Nature of the Band Gap of Halide Perovskites ABX3 (A = CH_3NH_3, Cs; B = Sn, Pb; X = Cl, Br, I): First-Principles Calculations. *Chin. Phys. B* **2015**, *24*, 116302.
(57) Jaroenjittichai, A. P.; Laosiritaworn, Y. Band Alignment of Cesium-Based Halide Perovskites. *Ceram. Int.* **2018**, *44*, S161−S163.
(58) Kang, Y.; Han, S. Intrinsic Carrier Mobility of Cesium Lead Halide Perovskites. *Phys. Rev. Appl.* **2018**, *10*, 044013.
(59) Qaid, S. M. H.; Ghaithan, H. M.; Al-Asbahi, B. A.; Aldwayyan, A. S. Tuning of Amplified Spontaneous Emission Wavelength for Green and Blue Light Emission through the Tunable Composition of $CsPb(Br_{1-x}Cl_x)_3$ Inorganic Perovskite Quantum Dots. *J. Phys. Chem. C* **2021**, *125*, 9441−9452.
(60) Akkerman, Q. A.; Motti, S. G.; Srimath Kandada, A. R.; Mosconi, E.; D'Innocenzo, V.; Bertoni, G.; Marras, S.; Kamino, B. A.; Miranda, L.; De Angelis, F.; et al. Solution Synthesis Approach to Colloidal Cesium Lead Halide Perovskite Nanoplatelets with Monolayer-Level Thickness Control. *J. Am. Chem. Soc.* **2016**, *138*, 1010−1016.

https://doi.org/10.1021/acsomega.1c04806
ACS Omega 2021, 6, 30752−30761

(61) Møller, C. K.; Sandor, E.; Wooster, W. A. Crystal Structure and Photoconductivity of Cæsium Plumbohalides. *Nature* **1958**, *182*, 1436.
(62) Sharma, S.; Halogen, X.; Erich, R. Phase Diagrams of Quasibinary Systems of the Type : ABX_3 A ' BX_3 ; ABX_3 AB ' X_3. *Z. Phys. Chem.* **1992**, *175*, 63−80.
(63) Liao, J.-F.; Rao, H.-S.; Chen, B.-X.; Kuang, D.-B.; Su, C.-Y. Dimension Engineering on Cesium Lead Iodide for Efficient and Stable Perovskite Solar Cells. *J. Mater. Chem. A* **2017**, *5*, 2066−2072.
(64) Rodová, M.; Brožek, J.; Knížek, K.; Nitsch, K. Phase Transitions in Ternary Caesium Lead Bromide. *J. Therm. Anal. Calorim.* **2003**, *71*, 667−673.
(65) Kirschner, M. S.; Diroll, B. T.; Guo, P.; Harvey, S. M.; Helweh, W.; Flanders, N. C.; Brumberg, A.; Watkins, N. E.; Leonard, A. A.; Evans, A. M.; et al. Photoinduced, Reversible Phase Transitions in All-Inorganic Perovskite Nanocrystals. *Nat. Commun.* **2019**, *10*, 504.
(66) Møller, C. K. *The Structure of Perovskite-Like Cæsium Plumbo Trihalides*; København Munksgaard, 1959; Vol *32*, p 2.
(67) Stoumpos, C. C.; Malliakas, C. D.; Peters, J. A.; Liu, Z.; Sebastian, M.; Im, J.; Chasapis, T. C.; Wibowo, A. C.; Chung, D. Y.; Freeman, A. J.; et al. Crystal Growth of the Perovskite Semiconductor $CsPbBr_3$: A New Material for High-Energy Radiation Detection. *Cryst. Growth Des.* **2013**, *13*, 2722−2727.
(68) Sutton, R. J.; Moore, D. T.; Kamino, B. A.; Patel, J. B.; Miranda, L.; Johnston, M. B.; Parrott, E. S.; Haghighirad, A. A.; Hörantner, M. T.; Snaith, H. J.; et al. Bandgap-Tunable Cesium Lead Halide Perovskites with High Thermal Stability for Efficient Solar Cells. *Adv. Energy Mater.* **2016**, *6*, 1502458.
(69) Eperon, G. E.; Paternò, G. M.; Sutton, R. J.; Zampetti, A.; Haghighirad, A. A.; Cacialli, F.; Snaith, H. J. Inorganic Caesium Lead Iodide Perovskite Solar Cells. *J. Mater. Chem. A* **2015**, *3*, 19688−19695.
(70) Wang, K.; Jin, Z.; Liang, L.; Bian, H.; Bai, D.; Wang, H.; Zhang, J.; Wang, Q.; Liu, S. All-Inorganic Cesium Lead Iodide Perovskite Solar Cells with Stabilized Efficiency beyond 15. *Nat. Commun.* **2018**, *9*, 4544.
(71) Marronnier, A.; Roma, G.; Boyer-Richard, S.; Pedesseau, L.; Jancu, J.-M.; Bonnassieux, Y.; Katan, C.; Stoumpos, C. C.; Kanatzidis, M. G.; Even, J. Anharmonicity and Disorder in the Black Phases of Cesium Lead Iodide Used for Stable Inorganic Perovskite Solar Cells. *ACS Nano* **2018**, *12*, 3477−3486.
(72) Momma, K.; Izumi, F. VESTA 3 for Three-Dimensional Visualization of Crystal, Volumetric and Morphology Data. *J. Appl. Crystallogr.* **2011**, *44*, 1272−1276.
(73) Parr, R. G. Density Functional Theory of Atoms and Molecules. *Horizons of Quantum Chemistry*; Springer, 1980; pp 5−15.
(74) Murnaghan, F. D. The Volume Changes of Five Gases under High Pressures. *J. Franklin Inst.* **1924**, *197*, 98.
(75) Paul, T.; Chatterjee, B. K.; Maiti, S.; Sarkar, S.; Besra, N.; Das, B. K.; Panigrahi, K. J.; Thakur, S.; Ghorai, U. K.; Chattopadhyay, K. K. Tunable Cathodoluminescence over the Entire Visible Window from All-Inorganic Perovskite $CsPbX_3$ 1D Architecture. *J. Mater. Chem. C* **2018**, *6*, 3322−3333.
(76) Sutton, R. J.; Filip, M. R.; Haghighirad, A. A.; Sakai, N.; Wenger, B.; Giustino, F.; Snaith, H. J. Cubic or Orthorhombic? Revealing the Crystal Structure of Metastable Black-Phase $CsPbI_3$ by Theory and Experiment. *ACS Energy Lett.* **2018**, *3*, 1787−1794.
(77) Trots, D. M.; Myagkota, S. V. High-Temperature Structural Evolution of Caesium and Rubidium Triiodoplumbates. *J. Phys. Chem. Solids* **2008**, *69*, 2520−2526.
(78) Cottingham, P.; Brutchey, R. L. On the Crystal Structure of Colloidally Prepared $CsPbBr_3$ Quantum Dots. *Chem. Commun.* **2016**, *52*, 5246−5249.
(79) Ghaithan, H. M.; Qaid, S. M. H.; Alahmed, Z. A.; Hezam, M.; Lyras, A.; Amer, M.; Aldwayyan, A. S. Anion Substitution Effects on the Structural, Electronic, and Optical Properties of Inorganic $CsPb(I_{1-x}Br_x)_3$ and $CsPb(Br_{1-x}Cl_x)_3$ Perovskites: Theoretical and Experimental Approaches. *J. Phys. Chem. C* **2021**, *125*, 886−897.
(80) Zhou, Y.; Zhao, Y. Chemical Stability and Instability of Inorganic Halide Perovskites. *Energy Environ. Sci.* **2019**, *12*, 1495−1511.
(81) Protesescu, L.; Yakunin, S.; Bodnarchuk, M. I.; Krieg, F.; Caputo, R.; Hendon, C. H.; Yang, R. X.; Walsh, A.; Kovalenko, M. V. Nanocrystals of Cesium Lead Halide Perovskites ($CsPbX_3$, X = Cl, Br, and I): Novel Optoelectronic Materials Showing Bright Emission with Wide Color Gamut. *Nano Lett.* **2015**, *15*, 3692−3696.
(82) Sun, P.-P.; Li, Q.-S.; Yang, L.-N.; Li, Z.-S. Theoretical Insights into a Potential Lead-Free Hybrid Perovskite: Substituting Pb^{2+} with Ge^{2+}. *Nanoscale* **2016**, *8*, 1503−1512.
(83) Zhang, P.; Zhu, G.; Shi, Y.; Wang, Y.; Zhang, J.; Du, L.; Ding, D. Ultrafast Interfacial Charge Transfer of Cesium Lead Halide Perovskite Films $CsPbX_3$ (X = Cl, Br, I) with Different Halogen Mixing. *J. Phys. Chem. C* **2018**, *122*, 27148−27155.
(84) Xiao, Z.; Yan, Y. Progress in Theoretical Study of Metal Halide Perovskite Solar Cell Materials. *Adv. Energy Mater.* **2017**, *7*, 1701136.
(85) Atourki, L.; Vega, E.; Mollar, M.; Marí, B.; Kirou, H.; Bouabid, K.; Ihlal, A. Impact of Iodide Substitution on the Physical Properties and Stability of Cesium Lead Halide Perovskite Thin Films $CsPbBr_{3-x}I_x (0 \le x \le 1)$. *J. Alloys Compd.* **2017**, *702*, 404−409.
(86) Liu, S.; Chen, G.; Huang, Y.; Lin, S.; Zhang, Y.; He, M.; Xiang, W.; Liang, X. Tunable Fluorescence and Optical Nonlinearities of All Inorganic Colloidal Cesium Lead Halide Perovskite Nanocrystals. *J. Alloys Compd.* **2017**, *724*, 889−896.
(87) Kang, B.; Biswas, K. Exploring Polaronic, Excitonic Structures and Luminescence in $Cs_4PbBr_6/CsPbBr_3$. *J. Phys. Chem. Lett.* **2018**, *9*, 830−836.
(88) Yu, J.; Liu, G.; Chen, C.; Li, Y.; Xu, M.; Wang, T.; Zhao, G.; Zhang, L. Perovskite $CsPbBr_3$ Crystals: Growth and Applications. *J. Mater. Chem. C* **2020**, *8*, 6326−6341 Royal Society of Chemistry May.
(89) Su, Y.; Chen, X.; Ji, W.; Zeng, Q.; Ren, Z.; Su, Z.; Liu, L. Highly Controllable and Efficient Synthesis of Mixed-Halide $CsPbX_3$ (X = Cl, Br, I) Perovskite QDs toward the Tunability of Entire Visible Light. *ACS Appl. Mater. Interfaces* **2017**, *9*, 33020−33028.
(90) Yin, W.-J.; Yan, Y.; Wei, S.-H. Anomalous Alloy Properties in Mixed Halide Perovskites. *J. Phys. Chem. Lett.* **2014**, *5*, 3625−3631.
(91) Qaid, S. M. H.; Ghaithan, H. M.; Al-Asbahi, B. A.; Alqasem, A.; Aldwayyan, A. S. Fabrication of Thin Films from Powdered Cesium Lead Bromide ($CsPbBr_3$) Perovskite Quantum Dots for Coherent Green Light Emission. *ACS Omega* **2020**, *5*, 30111−30122.
(92) Qaid, S. M. H.; Ghaithan, H. M.; Al-Asbahi, B. A.; Aldwayyan, A. S. Single-Source Thermal Evaporation Growth and the Tuning Surface Passivation Layer Thickness Effect in Enhanced Amplified Spontaneous Emission Properties of $CsPb(Br_{0.5}Cl_{0.5})_3$ Perovskite Films. *Polymers* **2020**, *12*, 2953.
(93) Jin, H.; Im, J.; Freeman, A. J. Topological Insulator Phase in Halide Perovskite Structures. *Phys. Rev. B: Condens. Matter Mater. Phys.* **2012**, *86*, 121102.
(94) Ilyas, B. M.; Elias, B. H. A Theoretical Study of Perovskite $CsXCl_3$ (X=Pb, Cd) within First Principles Calculations. *Phys. Rev. B: Condens. Matter Mater. Phys.* **2017**, *510*, 60−73.
(95) Yi, Z.; Fang, Z. Theoretical Studies on the Structural, Electronic and Optical Properties of Orthorhombic Perovskites $CH_3NH_3PbX_3$(X = I, Br, Cl). *J. Phys. Chem. Solids* **2017**, *110*, 145−151.
(96) Ghaithan, H. M.; Alahmed, Z. A.; Lyras, A.; Qaid, S. M. H.; Aldwayyan, A. S. Computational Investigation of the Folded and Unfolded Band Structure and Structural and Optical Properties of $CsPb(I_{1-x}Br_x)_3$ Perovskites. *Crystals* **2020**, *10*, 342.
(97) Ghaithan, H. M.; Alahmed, Z. A.; Qaid, S. M. H.; Aldwayyan, A. S. Structural, Electronic, and Optical Properties of $CsPb(Br_{1-x}Cl_x)_3$ Perovskite: First-Principles Study with PBE−GGA and MBJ−GGA Methods. *Materials* **2020**, *13*, 4944.
(98) Reshak, A. H.; Alahmed, Z. A.; Bila, J. Phase Transition in BaThO3 from Pbnm to Ibmm Turn the Fundamental Energy Band Gap from Indirect to Direct. *J. Alloys Compd.* **2019**, *771*, 607−613.
(99) William, D.; Callister, J. D. G. R. *Fundamentals of Materials Science and Engineering*, 4th ed; Hohn Wiley & Sons, Inc., 2012; pp 1−1087.
(100) Pitriana, P.; Wungu, T. D. K.; Herman; Hidayat, R. The Characteristics of Band Structures and Crystal Binding in All-Inorganic Perovskite $APbBr_3$ Studied by the First Principle Calculations Using the

https://doi.org/10.1021/acsomega.1c04806
ACS Omega 2021, 6, 30752−30761

Density Functional Theory (DFT) Method. *Results Phys.* **2019**, *15*, 102592.
(101) Benchehima, M.; Abid, H.; Sadoun, A.; Chabane Chaouche, A. Optoelectronic Properties of Aluminum Bismuth Antimony Ternary Alloys for Optical Telecommunication Applications: First Principles Calculation. *Comput. Mater. Sci.* **2018**, *155*, 224−234.
(102) Ghebouli, M. A.; Ghebouli, B.; Fatmi, M. First-Principles Calculations on Structural, Elastic, Electronic, Optical and Thermal Properties of $CsPbCl_3$ Perovskite. *Phys. Rev. B: Condens. Matter Mater. Phys.* **2011**, *406*, 1837−1843.
(103) Kushwaha, A. K.; Laref, A.; Laref, S. First-Principles Investigation of Structural, Electronic, Optical, and Magnetic Properties of Ternary Mixed Compound $CsTe_xS_{1-x}$. *J. Electron. Mater.* **2019**, *48*, 3479−3489.
(104) Narsimha Rao, E.; Vaitheeswaran, G.; Reshak, A. H.; Auluck, S. Role of Spin-Orbit Interaction on the Nonlinear Optical Response of $CsPbCO_3F$ Using DFT. *Phys. Chem. Chem. Phys.* **2017**, *19*, 31255−31266.
(105) Wu, Z.; Cohen, R. E. More Accurate Generalized Gradient Approximation for Solids. *Phys. Rev. B: Condens. Matter Mater. Phys.* **2006**, *73*, 235116.

https://doi.org/10.1021/acsomega.1c04806
ACS Omega 2021, 6, 30752−30761